


Curcumin Coated Ultra-Small Iron Oxide Nanoparticles as T_1 Contrast Agents for Magnetic Resonance Imaging of Cancer Cells

Azadeh Amraee (PhD Candidate)^{1*}, Abolfazl Sarikhani (MSc)², Leili Darvish (PhD Candidate)³, Zahra Alamzadeh (MSc)², Rasoul Irajirad (MSc)², Seyed Rabie Mahdavi (PhD)¹

ABSTRACT

Background: The application of nanotechnology in the molecular diagnosis and treatment of cancer is essential.

Objective: This study aimed to investigate the influence of curcumin-coated ultra-small superparamagnetic iron oxide (USPIO) as a T_1 contrast agent in Magnetic Resonance Imaging (MRI).

Material and Methods: In this experimental study, the influence of curcumin-coated USPIO ($Fe_3O_4@C$) on the diagnosis of the cancer cell line was investigated. After synthesis, characterization, and relaxation of $Fe_3O_4@C$, the contrast changes in T_1 -weight MRI to mouse colon carcinoma 26 cell line were evaluated in vitro.

Results: $Fe_3O_4@C$ nanoparticles (NPs) are good at imaging; based on a relaxometry test, the r_1 and r_2 relaxivities of Dotarem were 3.139 and 0.603 $mM^{-1}s^{-1}$, respectively. Additionally, the r_1 and r_2 relaxivities of $Fe_3O_4@C$ were 3.792 and 1.3 $mM^{-1}s^{-1}$, respectively, with the rate of 2.155 of r_2/r_1 NPs.

Conclusion: The NPs can be identified as a positive contrast agent with a weight of T_1 in MRI. The core-shell $Fe_3O_4@C$ NPs can be effective in cancer treatment and diagnosis because of the therapeutic effects of curcumin and the properties of USPIO.

Citation: Amraee A, Sarikhani A, Darvish L, Alamzadeh Z, Irajirad R, Mahdavi SR. Curcumin Coated Ultra-Small Iron Oxide Nanoparticles as T_1 Contrast Agents for Magnetic Resonance Imaging of Cancer Cells. *J Biomed Phys Eng.* 2024;14(5):447-456. doi: 10.31661/jbpe.v0i0.2201-1447.

Keywords

Ultra-small Iron Oxide; Nanoparticles; Curcumin; Magnetic Resonance Imaging; Contrast Agent

Introduction

One of the most critical factors in the revolutionary transformation of technology and science is metal oxide nanoparticles. Ultra-small iron oxides are recently used in biomedicine among the many metal oxides. Numerous ways have been developed to produce magnetic nanoparticles by controlling their shapes, sizes, and distribution [1-3]. The high surface-to-volume ratio and bipolar-dipole interaction cause magnetic nanoparticles to accumulate more than non-magnetic nanoparticles. Particles can be stable in two ways, by either electrostatic stabilization or spatial stabilization, achieved by attaching long-chain surfactants to the surface of nanoparticles to avoid from nearby. Scatter stabilization is attained by applying a surface charge on

¹Department of Medical Physics, Iran University of Medical Sciences, Tehran, Iran

²Finetech in Medicine Research Center, Iran University of Medical Sciences, Tehran, Iran

³Department of Medical Physics, Faculty of Medicine, Mashhad University of Medical Sciences, Mashhad, Iran

*Corresponding author:
Azadeh Amraee
Department of Medical Physics, Iran University of Medical Sciences, Tehran, Iran
E-mail: amraee.gelare@yahoo.com

Received: 8 January 2022
Accepted: 20 February 2022

the nanoparticles, leading to electrostatic repulsion of the particles. Curcumin, a yellow polyphenolic compound originating in the rhizomes of turmeric, is recognized for its anti-cancer, anti-microbial, and anti-inflammation activities, leading it a favorable candidate for iron oxide covering. Curcumin coating is reported on iron oxide nanoparticles (IONPs) with bonds, such as oleic acid, chitosan, and silica [4]. After undergoing synthesis, modification, and final modulation steps, magnetic nanoparticles lead to the production of valuable materials for the diagnosis and treatment of disease. Magnetic Resonance Imaging (MRI) is one of the most widely used diagnostic tools due to its special features, such as non-invasiveness, non-ionization, no restriction on tissue penetration, high soft-tissue contrast, and high spatial resolution.

However, considering the low contrast sensitivity in cancer tissues, MRI needs to use contrast agents [5]. In general, contrast agents are allocated into T_1 and T_2 weighted contrast. Positive (or bright) contrast enhancement can be attained by T_1 weighted contrast, and negative (or dark) contrast improvement can be produced by T_2 weighted contrast, causing protons in their neighborhood to undergo spin-spin relaxation [6]. T_1 contrast agents are preferred due to the drawbacks of T_2 weighted images, such as incorrect signals from areas of calcification and metal deposition [7]. Most of the approved T_1 weighted contrast, like Dotarem (gadoterate meglumine), are based on Gd^{+3} paramagnetic ions [8]. Recent studies have shown [9] that gadolinium compounds form a potent complex with bio-ligands and increase the potential for toxicity. Some gadolinium is found in patients' brains depending on the dose received [10]. The Food and Drug Administration (FDA) issues a general caution for all gadolinium-based substances and prohibits their use in patients with acute renal failure. The use of these compounds is expected to be phased out shortly. Some studies are conducted to develop T_1 alternative

contrast materials [6, 7]. Magnetic iron oxide nanoparticles (NPs), commonly used as a T_2 contrast agent, have recently been potential T_1 contrast agents when their size decreases. The physical properties of iron oxide depend on the size of the iron. When the size of iron oxide is less than 5 nm due to volume reduction, magnetic anisotropy, and spin tilt, the property of iron oxide changes from superparamagnetic to paramagnetic state. Therefore, reducing the size of the particles changes them from T_2 into T_1 contrast agents [11-18]. These magnetic IONPs can demonstrate excellent T_1 contrast performance by a large surface area with five unpaired electrons in the iron ion. Compared to gadolinium-based contrast agents, IONPs agents are more compatible since iron is a necessary element in the human body [19]. However, the use of IONPs as T_1 contrast material is still an important challenge. In addition, IONPs lead to an increase in T_2 contrast and the fading of T_1 contrast since they tend to form collections under physiological conditions [20]. Some studies are conducted to alter the surface of iron oxide nanoparticles through various methods [21-23]. This study aimed to synthesize superparamagnetic iron oxide (USPIO) with curcumin coating and also investigate MR imaging parameters, such as r_1 and r_2/r_1 , to use these nanoparticles as a positive contrast agent compared to gadolinium-based clinical Dotarem.

Material and Methods

This study is an experimental type of study.

1. Synthesis and characterization of curcumin covered iron oxide nanoparticles

1.1. Nanoparticles' Synthesis

Curcumin Coated USPIO NPs synthesis to a combination of 20 ml of iron precursor solution (0.05 M $FeCl_2 \cdot 4H_2O$ and 0.1 M $FeCl_3 \cdot 6H_2O$) liquefied in water was added dropwise 100 ml of 10 N ammonium hydroxide that 0.5 g curcumin was dissolved in its under-nitrogen

atmosphere. The product was stirred for about 60 min in a water bath at 80 °C for whole formation magnetite particles. The resulting stable solution was cooled to room temperature and dialyzed against water in a cellulose membrane for 3 days to eliminate extra curcumin, followed by drying in a vacuum oven at 50 °C and attaining the product. The primary characterization displays that the phenolic and enolic OH of the curcumin was used in binding with nanoparticles.

1.2. Characterization

A transmission electron microscope (TEM; LEO 906; Zeiss) at an acceleration voltage of 100 kV was used to determine the morphology and size distribution of the synthesized NPs. The hydrodynamic diameter of NPs and surface charge (zeta potential) were measured by dynamic light scattering (DLS; Malvern Zetasizer Nano ZS-90). The absorption spectra of water-dispersed NPs were recorded using a UV visible spectrophotometer (UV-2600, Shimadzu, Japan).

2. Cell culture

This study was conducted on murine undifferentiated colon carcinoma cell lines acquired from the Pasteur Institute of Iran. Mouse colon carcinoma 26 (CT26) cell line was cultured under controlled conditions and in vitro. The cells were cultured as monolayers in RPMI-1640 cell culture media with L-glutamine and NaHCO_3 , 100 $\mu\text{g}/\text{mL}$ streptomycin, 10% FBS, and (100 U/ml) penicillin; cells were harvested after reaching nearly 80% confluence with trypsin / EDTA 0.25%.

3. MTT assay

Cells were seeded in 96-well plates with 10^4 cells per well and retained in an incubator at 37 °C and 5% CO_2 overnight to evaluate the cytotoxicity of NPs on cell lines. After draining the contents of the wells, 100 ml of culture medium and NPs with different concentrations were added to each well and incubated for 4 and 24 h. 100 μl of 3-(4,5-dimethylthi-

azol-2-yl)-2, 5-diphenyltetrazolium bromide (MTT) solution was added to each sample after the incubation period. Re-incubation was done for 4 h; the surface of the wells was then emptied. The samples were rewashed, and 100 μl of dimethyl sulfoxide (DMSO) was added to each well. The absorption of the optical color was determined by the Enzyme-Linked Immunosorbent Assay (ELISA) reader at 570 nm. Finally, the optimal concentration for diagnosis was determined using the cell survival percentage obtained with the MTT assays.

4. MRI Imaging

The time of relaxation was measured with MRI. The water was used to prepare concentrations of the NPs, and the microtubes were put in the water phantom in order of concentration. The spin-echo protocol was used to perform the image; the amount of signal change in T_1 of the sample was determined using a Time Echo (TE) (14 ms) with different Repetition Time (TR)s (100, 300, 600, 1000, 2000, 3000, and 5000 ms). A fixed TR (600 ms) with several echoes with different TEs (14, 28, 44, 58, 86, 100, 158, and 200 ms) was used to determine the signal reduction in the T_2 of the sample. SPSS software (version 20) was used to determine the signal intensity for each concentration, and signal graphs were plotted in terms of different TRs and TEs for each concentration. Using the values obtained from the previous steps does not appear to be modifying the subject graphs $1/T_1$ and $1/T_2$ in terms of concentration using SPSS software, and the values of r_1 and r_2 were obtained.

4.1. Determine SNR and ΔSNR parameters

Cellular uptake of NPs and Dotarem was examined by in vitro imaging of the phantom, and CT26 cells were cultured in T75 flasks and incubated with $\text{Fe}_3\text{O}_4@\text{C}$ and Dotarem at a concentration of 0.25, 0.1, 0.2, 0.5, and 1 mM for 24 h. The cells were washed with Phosphate-buffered saline (PBS), fixed in 2% agar gel, and placed in Eppendorf tubes.

The control group included cell-free agar gel. Signal noise ratio (SNR) and Signal to noise ratio-delta (Δ SNR) were obtained using the equations (1) and (2) as follows:

$$SNR = \frac{SI_{mean}}{SD_{noise}} \quad (1)$$

$$\Delta SNR = \frac{SNR_{post} - SNR_{pre}}{SNR_{pre}} \times 100 \quad (2)$$

Where SI mean is the average signal intensity in a sample of the contrast agent, and

SD noise is the average standard deviation of the field. Further, SNR post is obtained by the contrast agent, and SNR pre is SNR obtained in water.

5. Statistical analysis

All tests were done in triplicate, and the data was stated as mean values \pm SD (standard deviation). One-way analysis of variance (ANOVA) followed by the Tukey test was performed a post hoc at a 95% confidence level to evaluate the importance of experimental data using SPSS software (version 16). P -value $<$ 0.05 was considered statistically significant.

Results

Characterization of Fe₃O₄@C

Physical properties of Fe₃O₄@C NPs were determined using DLS and Zeta potential. An electron microscope examined the shape and size of the NPs. The dynamic light scattering was used to measure the diameter of NPs and their surface charge. TEM images showed that Fe₃O₄@C nanoparticles have an average size of 3.5 nm. The hydrodynamic diameter of NPs using the DLS test was 12.73 nm. Their surface charge (zeta potential) was -13 mV. Based on the results of UV-visible spectra, Fe₃O₄@C increased absorption in the range of 420 nm (Figure 1) [24].

Cellular toxicity evaluation MTT assay

CT26 cells were exposed to different

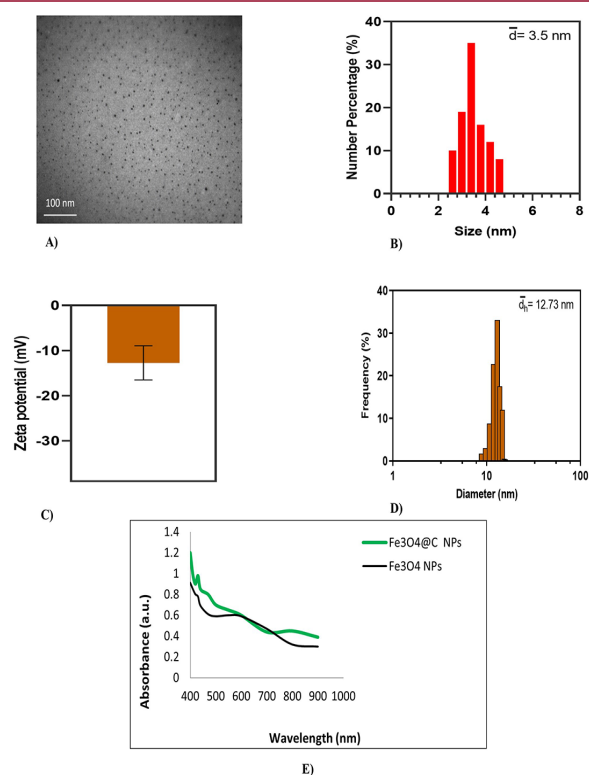


Figure 1: Transmission electron microscope (TEM) images (A), size distribution histogram (B), Zeta potential (C), Dynamic light scattering (D) and UV-visible spectra (E) of Fe₃O₄@C NPs

concentrations of NPs, and Dotarem included 0.02, 0.05, 0.1, 0.3, 0.5, 1, and 2 Mm and incubated for 4 and 24 h to evaluate their toxicity by MTT assay. As shown in the diagrams (Figure 2), at all concentrations and 4 and 24 h incubation, the toxicity of Fe₃O₄@C nanoparticles is less than that of Dotarem; the process of decreasing cell survival was very slow at concentrations lower than 2 mm (Figure 2). The data shows the average of the results of three trials (\pm standard error).

Relaxation rates and MRI performances of Fe₃O₄@C and Dotarem

Relaxometry with 3 Tesla fields (SIEMENS, MAGNETOM Prisma, Germany) in concentrations of 0.025, 0.05, 0.1, 0.2, 0.5, and 1 mM was used to investigate the possibility of using Fe₃O₄@C as a T₁ MRI contrast

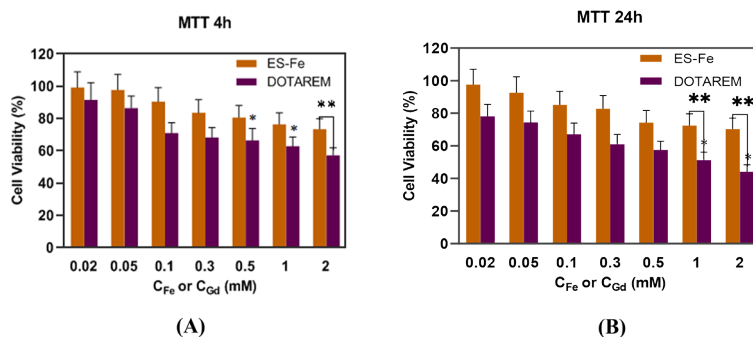


Figure 2: The 3-(4,5dimethylthiazol-2-yl)-2, 5-diphenyltetrazolium bromide (MTT) assay results of Mouse colon carcinoma 26 (CT26) cell lines which were treated with Fe₃O₄@C and Dotarem in different incubation times; 4 h (A), 24 h (B). (*significant difference with the control group, **significant difference of Fe₃O₄@C and Dotarem a specific concentration P -value<0.05).

agent. The longitudinal (r_1) and transverse (r_2) molar relaxivities were considered according to the equation of $r = \Delta(1/T) / \Delta[Fe]$. The r_1 and r_2 relaxivities of Dotarem were 3.139 and 0.603 mM⁻¹s⁻¹. Moreover, r_1 and r_2 relaxivities of Fe₃O₄@C were 3.792 and 1.3 mM⁻¹s⁻¹ (Figure 3). Corresponding to r_2/r_1 ratios of Dotarem and Fe₃O₄@C were 1.208 and 2.155,

respectively (Table 1). The low r_2/r_1 ratios (below 5) of Fe₃O₄@C NPs confirmed that they are sufficient for T₁-weighted contrast agents and comparable to clinical Dotarem.

In Vitro MR Imaging

In vitro MRI to assess performance, the contrast enhancement properties, and relaxation times (T) of Fe₃O₄@C and Dotarem in an aqueous solution with diverse concentrations were determined on a 3 T MRI scanner. T₁ weighted images of CT26 cells treated with Fe₃O₄@C and Dotarem at concentrations of 0.25, 0.1, 0.2, 0.5, and 1 mM were used. As indicated in Figure 4, for the T₁ phantom images, both Fe₃O₄@C and Dotarem demonstrated brightening contrast enhancement with the increasing concentration, showing that they were T₁ contrast agents at these concentrations and our synthesis NP can be a positive contrast agent. The amounts of Δ SNR in the CT26 cell line treated with Dotarem at

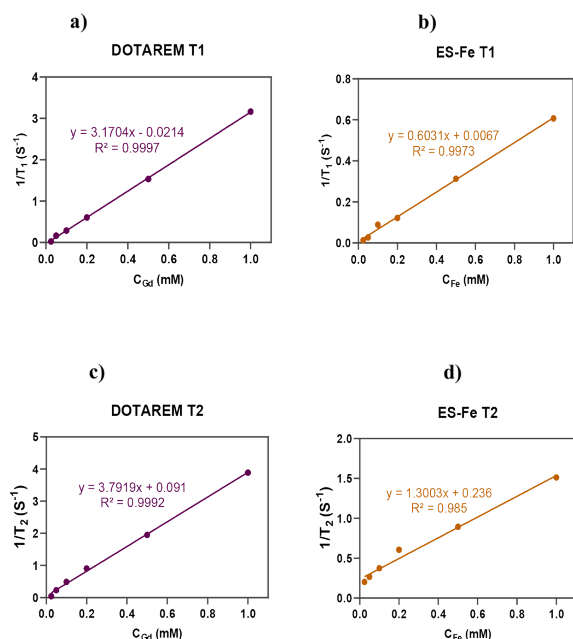


Figure 3: (a) Plot of $1/T_1$ of Dotarem, (b) Plot of $1/T_1$ over Fe concentration of Fe₃O₄@C, (c) Plot of $1/T_2$ of Dotarem, (d) Plot of $1/T_2$ over Fe concentration of Fe₃O₄@C

Table 1: Relaxometry of clinical Dotarem and Fe₃O₄@C in Tesla field 3

	Sample	r_1	r_2	r_2/r_1
1	DOTAREM	3.139	3.792	1.208
2	Fe ₃ O ₄ @C	0.603	1.3	2.155

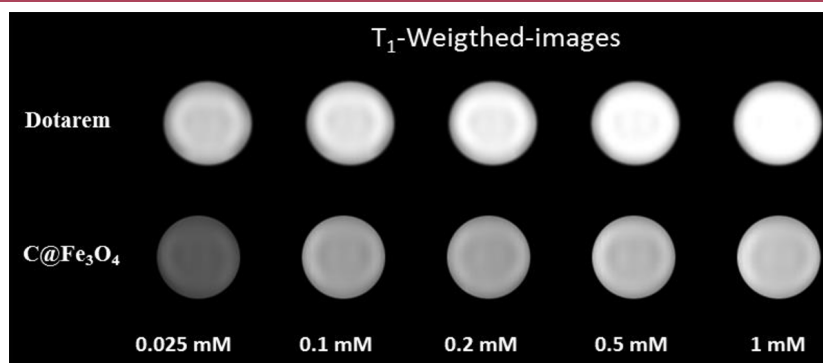


Figure 4: T_1 weighted Magnetic Resonance images (T_1 -W MRI) of Mouse colon carcinoma 26 (CT26) cell pellets after 24 h incubation with $Fe_3O_4@C$ and Dotarem at concentrations of 0.25, 0.1, 0.2, 0.5, and 1 mM (Time Echo (TE)=12 and Repetition Time (TR)=600 ms).

concentrations of 1, 0.5, 0.2, 0.1, and 0.25 mM, consisted of 160.8 ± 1.1 , 153.8 ± 1 , 101 ± 2.2 , 60.21 ± 1.1 , and 30.05 ± 1.3 , respectively. Further, these amounts in CT26 cell lines treated with $Fe_3O_4@C$ NPs consisted of 80.21 ± 1.3 , 53.21 ± 1.1 , 47.41 ± 1.2 , 35.93 ± 1 , and 20.4 ± 2.2 , respectively (Figure 5).

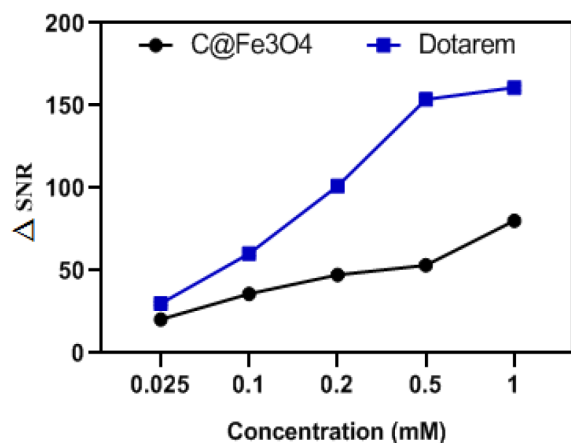


Figure 5: Signal to noise ratio-delta (Δ SNR) in T_1 weighted Magnetic Resonance images (T_1 -W MRI) with (Time Echo (TE)=12 and Repetition Time (TR)=600 ms) of Mouse colon carcinoma 26 (CT26) cell lines, which were treated with $Fe_3O_4@C$ and Dotarem in different concentrations of 1, 0.5, 0.2, 0.1, and 0.25 mM and an incubation time of 24 hours.

Discussion

Among a wide range of NPs, iron oxide NPs have considered important due to their unique properties [25]. Iron oxide NPs larger than 10 nm are known as negative contrast agents; lately, NPs smaller than 5 nm are recognized as positive contrast agents [11], showing the best size for iron oxide NPs for T_1 weighted MRI is 3.6 nm [26]. The formation of these NPs can be seen in the TEM images of the synthesis of $Fe_3O_4@C$. The size of $Fe_3O_4@C$ NPs was about 3.5 nm (Figure 1 A). The main reason for the contrast is that different levels of water protons in different organs result in other relaxation times. Iron oxide NPs reduce the relaxation time of T_1 and T_2 water protons in different organs and contrast in MRI [26]. As shown in Figure 4, T_1 map images showed that Fe concentration directly affects the relaxation rate of the water protons and, consequently, the contrast [27]. Moreover, if the rate of contrast agent in r_2/r_1 is less than 5, it is known as a contrast agent with a weight of T_1 . The ratio is recently reduced to 2 [28]. Based on Shen et al. study conducted on iron oxide NPs for T_1 weighted MRI (5 nm), the r_1 and r_2/r_1 ratio was 70 and $1.98 \text{ mM}^{-1}\text{s}^{-1}$, respectively. MR images confirmed that the synthesized nanoparticles were positive contrast agents [29]. Park et al. synthesized

Polyethylene glycol) PEG (-coated iron oxide NPs for T_1 weighted MRI (3 nm), and the r_1 and r_2/r_1 ratio was 3.1 and 5.6 $\text{mM}^{-1}\text{s}^{-1}$, respectively [30]. In the present study, relaxometry was used to obtain the parameters r_1 and r_2 for curcumin-coated iron oxide NPs. The r_1 , r_2 , and r_2/r_1 ratio of $\text{Fe}_3\text{O}_4@\text{C}$ was 0.603 $\text{mM}^{-1}\text{s}^{-1}$, 1.2 $\text{mM}^{-1}\text{s}^{-1}$, and 2.155, respectively. The data attained from this study is comparable to clinical Dotarem (Table 1). USPIO NPs have small amounts of r_1 combined with gadolinium oxide or gadolinium particles to solve this problem [26]. The diagnostic and therapeutic applications of magnetic NPs in the body can be affected by the use of selective coating. Curcumin conjugates NPs to increase its therapeutic effects is considered by many researchers [31-33]. Curcumin is a well-studied natural compound due to its cancer inhibition and anti-cancer activities influenced by multiple signaling pathways. In addition, enhancing the uptake in cancer cells and improving the therapeutic effects of curcumin were demonstrated by the NPs loaded with curcumin. Fengxia Li et al. used polylactic acid to load curcumin in 2011 [34]. The researchers used methods for creating magnetic fluids by coating nanoparticles with Dextran and pluronic polymer and loading curcumin. This study aimed to release curcumin, an anti-cancer agent, and produce a contrast agent in MRI [35]. Ning Wang et al. used PEO-PPO-PEO copolymers to coat nanoparticles and curcumin in coated nanoparticle structures [36]. Kwok Kin Ch et al. loaded curcumin into the structure of magnetic nanoparticles coated with polyethylene glycol and polylactic [37]. In addition, Mankala et al. introduced curcumin into magnetic nanoparticles coated with dextran and polylysine [38]. In the present study, the surface of Fe_3O_4 nanoparticles synthesized using citric acid (CA) was modified to bind into curcumin without the use of any polymer coating. Studies indicate that if the r_2/r_1 content is less than 5, the contrast agent is known as the T_1 weighted contrast agent. The

data suggest that the nanoparticle synthesized in the present study could be identified as a positive contrast agent. Curcumin can also be used as a potential therapeutic agent due to its anti-cancer properties.

Conclusion

$\text{Fe}_3\text{O}_4@\text{C}$ NPs were synthesized by coprecipitation of iron ions and subsequently covered with curcumin. The NPs were characterized by TEM, DLS, and Zeta potential techniques. TEM images showed $\text{Fe}_3\text{O}_4@\text{C}$ nanoparticles have an average size of 3.5 nm, and the hydrodynamic diameter of MNP was 12.73 nm using the DLS test. The data relating to the parameters r_1 , r_2 , and r_2/r_1 were 0.603, 1.3, and 2.155, respectively. $\text{Fe}_3\text{O}_4@\text{C}$ NPs are promising magnetic NPs that may be concurrently used as a T_1 assessment agent in MRI, magnetically targeted drug delivery systems, and biomedical applications. Further research could help extend this method for preclinical and clinical use. According to the results, $\text{Fe}_3\text{O}_4@\text{C}$ NPs can have the potential for further evaluation for diagnostic and treatment purposes.

Acknowledgment

This study was supported by the Iran University of Medical Sciences Ph.D. candidate project grant (Ms. Azadeh Amraee, grant number: 16122) financially.

Authors' Contribution

A. Amraee performed all in vitro experiments, analyzed the data, and wrote the manuscript. A. Sarikhani performed MR imaging. R. Irajirad synthesized the nanoparticles. L. Darvish and Z. Alamzadeh contributed to the concept and design. SR. Mahdavi, supervising the data analyses and final approval of the manuscript. All authors read and approved the final manuscript.

Ethical Approval

Ethical approval was obtained by the

Ethics Committee of our University (Ethics code: IR.IUMS.FMD.REC.1398.420).

Conflict of Interest

None

References

- Mosayebi J, Kiyasatfar M, Laurent S. Synthesis, functionalization, and design of magnetic nanoparticles for theranostic applications. *Adv Healthc Mater.* 2017;**6**(23):1700306. doi: 10.1002/adhm.201700306. PubMed PMID: 28990364.
- Jabbar KQ, Barzinjy AA, Hamad SM. Iron oxide nanoparticles: Preparation methods, functions, adsorption and coagulation/flocculation in wastewater treatment. *Environmental Nanotechnology, Monitoring & Management.* 2022;**17**:100661. doi: 10.1016/j.enmm.2022.100661.
- Hooshmand S, Hayat SMG, Ghorbani A, Khatami M, Pakravanan K, Darroudi M. Preparation and Applications of Superparamagnetic Iron Oxide Nanoparticles in Novel Drug Delivery Systems: An Overview. *Curr Med Chem.* 2021;**28**(4):777-99. doi: 10.2174/0929867327666200123152006. PubMed PMID: 31971104.
- Onoue S, Takahashi H, Kawabata Y, Seto Y, Hatanaka J, Timmermann B, et al. Formulation design and photochemical studies on nanocrystal solid dispersion of curcumin with improved oral bioavailability. *J Pharm Sci.* 2010;**99**(4):1871-81. doi: 10.1002/jps.21964. PubMed PMID: 19827133.
- Strijkers GJ, Mulder WJ, Van Tilborg GA, Nicolay K. MRI contrast agents: current status and future perspectives. *Anticancer Agents Med Chem.* 2007;**7**(3):291-305. doi: 10.2174/187152007780618135. PubMed PMID: 17504156.
- Villaraza AJ, Bumb A, Brechbiel MW. Macromolecules, dendrimers, and nanomaterials in magnetic resonance imaging: the interplay between size, function, and pharmacokinetics. *Chem Rev.* 2010;**110**(5):2921-59. doi: 10.1021/cr900232t. PubMed PMID: 20067234. PubMed PMCID: PMC2868950.
- Tao C, Zheng Q, An L, He M, Lin J, Tian Q, et al. T1-Weight Magnetic Resonance Imaging Performances of Iron Oxide Nanoparticles Modified with a Natural Protein Macromolecule and an Artificial Macromolecule. *Nanomaterials.* 2019;**9**(2):170. doi: 10.3390/nano9020170. PubMed PMID: 30704072. PubMed PMCID: PMC6409807.
- Bellin MF, Van Der Molen AJ. Extracellular gadolinium-based contrast media: an overview. *Eur J Radiol.* 2008;**66**(2):160-7. doi: 10.1016/j.ejrad.2008.01.023. PubMed PMID: 18358659.
- Blomqvist L, Nordberg GF, Nurchi VM, Aaseth JO. Gadolinium in Medical Imaging-Usefulness, Toxic Reactions and Possible Countermeasures-A Review. *Biomolecules.* 2022;**12**(6):742. doi: 10.3390/biom12060742. PubMed PMID: 35740867. PubMed PMCID: PMC9221011.
- Ramalho J, Semelka RC, Ramalho M, Nunes RH, AIObaidy M, Castillo M. Gadolinium-Based Contrast Agent Accumulation and Toxicity: An Update. *AJNR Am J Neuroradiol.* 2016;**37**(7):1192-8. doi: 10.3174/ajnr.A4615. PubMed PMID: 26659341. PubMed PMCID: PMC7960350.
- Tromsdorf UI, Bruns OT, Salmen SC, Beisiegel U, Weller H. A highly effective, nontoxic T1 MR contrast agent based on ultrasmall PEGylated iron oxide nanoparticles. *Nano Lett.* 2009;**9**(12):4434-40. doi: 10.1021/nl902715v. PubMed PMID: 19799448.
- Kim BH, Lee N, Kim H, An K, Park YI, Choi Y, et al. Large-scale synthesis of uniform and extremely small-sized iron oxide nanoparticles for high-resolution T1 magnetic resonance imaging contrast agents. *J Am Chem Soc.* 2011;**133**(32):12624-31. doi: 10.1021/ja203340u. PubMed PMID: 21744804.
- Shen Z, Wu A, Chen X. Iron oxide nanoparticle based contrast agents for magnetic resonance imaging. *Molecular Pharmaceutics.* 2017;**14**(5):1352-64.
- Lee N, Yoo D, Ling D, Cho MH, Hyeon T, Cheon J. Iron Oxide Based Nanoparticles for Multimodal Imaging and Magneto-responsive Therapy. *Chem Rev.* 2015;**115**(19):10637-89. doi: 10.1021/acs.chemrev.5b00112. PubMed PMID: 26250431.
- Rui Y-P, Liang B, Hu F, Xu J, Peng Y-F, Yin P-H, et al. Ultra-large-scale production of ultrasmall superparamagnetic iron oxide nanoparticles for T1-weighted MRI. *RSC advances.* 2016;**6**(27):22575-85. doi: 10.1039/c6ra00347h.
- Luo Y, Yang J, Yan Y, Li J, Shen M, Zhang G, Mignani S, Shi X. RGD-functionalized ultrasmall iron oxide nanoparticles for targeted T1-weighted MR imaging of gliomas. *Nanoscale.* 2015;**7**(34):14538-46. doi: 10.1039/c5nr04003e. PubMed PMID: 26260703.
- Liu CL, Peng YK, Chou SW, Tseng WH, Tseng YJ, Chen HC, et al. One-step, room-temperature synthesis of glutathione-capped iron-oxide nanoparticles and their application in in vivo T1-weighted magnetic resonance imaging. *Small.* 2014;**10**(19):3962-

9. doi: 10.1002/sml.201303868. PubMed PMID: 25044378.
18. Huang J, Wang L, Zhong X, Li Y, Yang L, Mao H. Facile non-hydrothermal synthesis of oligosaccharides coated sub-5 nm magnetic iron oxide nanoparticles with dual MRI contrast enhancement effect. *J Mater Chem B*. 2014;**2**(33):5344-51. doi: 10.1039/C4TB00811A. PubMed PMID: 25181490. PubMed PMCID: PMC4147377.
19. Liu G, Gao J, Ai H, Chen X. Applications and potential toxicity of magnetic iron oxide nanoparticles. *Small*. 2013;**9**(9-10):1533-45. doi: 10.1002/sml.201201531. PubMed PMID: 23019129.
20. Wang L, Huang J, Chen H, Wu H, Xu Y, Li Y, Yi H, et al. Exerting Enhanced Permeability and Retention Effect Driven Delivery by Ultrafine Iron Oxide Nanoparticles with T1-T2 Switchable Magnetic Resonance Imaging Contrast. *ACS Nano*. 2017;**11**(5):4582-92. doi: 10.1021/acsnano.7b00038. PubMed PMID: 28426929. PubMed PMCID: PMC5701890.
21. Xiao L, Li J, Brougham DF, Fox EK, Feliu N, Bushmelev A, et al. Water-soluble superparamagnetic magnetite nanoparticles with biocompatible coating for enhanced magnetic resonance imaging. *ACS Nano*. 2011;**5**(8):6315-24. doi: 10.1021/nn201348s. PubMed PMID: 21790153.
22. Wang G, Zhang X, Skallberg A, Liu Y, Hu Z, Mei X, Uvdal K. One-step synthesis of water-dispersible ultra-small Fe₃O₄ nanoparticles as contrast agents for T1 and T2 magnetic resonance imaging. *Nanoscale*. 2014;**6**(5):2953-63. doi: 10.1039/c3nr05550g. PubMed PMID: 24480995.
23. Hu Y, Mignani S, Majoral JP, Shen M, Shi X. Construction of iron oxide nanoparticle-based hybrid platforms for tumor imaging and therapy. *Chem Soc Rev*. 2018;**47**(5):1874-900. doi: 10.1039/c7cs00657h. PubMed PMID: 29376542.
24. Cheng KK, Chan PS, Fan S, Kwan SM, Yeung KL, et al. Curcumin-conjugated magnetic nanoparticles for detecting amyloid plaques in Alzheimer's disease mice using magnetic resonance imaging (MRI). *Biomaterials*. 2015;**44**:155-72. doi: 10.1016/j.biomaterials.2014.12.005. PubMed PMID: 25617135.
25. Lu M, Ozcelik A, Grigsby CL, Zhao Y, Guo F, Leong KW, Huang TJ. Microfluidic Hydrodynamic Focusing for Synthesis of Nanomaterials. *Nano Today*. 2016;**11**(6):778-92. doi: 10.1016/j.nantod.2016.10.006. PubMed PMID: 30337950. PubMed PMCID: PMC6191180.
26. Shen Z, Chen T, Ma X, Ren W, Zhou Z, Zhu G, et al. Multifunctional Theranostic Nanoparticles Based on Exceedingly Small Magnetic Iron Oxide Nanoparticles for T1-Weighted Magnetic Resonance Imaging and Chemotherapy. *ACS Nano*. 2017;**11**(11):10992-1004. doi: 10.1021/acsnano.7b04924. PubMed PMID: 29039917.
27. Nejadshafiee V, Naeimi H, Goliaei B, Bigdeli B, Sadighi A, Dehghani S, et al. Magnetic bio-metal-organic framework nanocomposites decorated with folic acid conjugated chitosan as a promising biocompatible targeted theranostic system for cancer treatment. *Mater Sci Eng C Mater Biol Appl*. 2019;**99**:805-15. doi: 10.1016/j.msec.2019.02.017. PubMed PMID: 30889755.
28. Demirer GS, Okur AC, Kizilel S. Synthesis and design of biologically inspired biocompatible iron oxide nanoparticles for biomedical applications. *J Mater Chem B*. 2015;**3**(40):7831-49. doi: 10.1039/c5tb00931f. PubMed PMID: 32262898.
29. Shen Z, Song J, Zhou Z, Yung BC, Aronova MA, Li Y, et al. Dotted Core-Shell Nanoparticles for T1 -Weighted MRI of Tumors. *Adv Mater*. 2018;**30**(33):1803163. doi: 10.1002/adma.201803163. PubMed PMID: 29972604. PubMed PMCID: PMC6320323.
30. Park EA, Lee W, So YH, Lee YS, Jeon BS, Choi KS, et al. Extremely Small Pseudoparamagnetic Iron Oxide Nanoparticle as a Novel Blood Pool T1 Magnetic Resonance Contrast Agent for 3 T Whole-Heart Coronary Angiography in Canines: Comparison With Gadoterate Meglumine. *Invest Radiol*. 2017;**52**(2):128-33. doi: 10.1097/RLI.0000000000000321. PubMed PMID: 27977466.
31. Yallapu MM, Jaggi M, Chauhan SC. Curcumin nanoformulations: a future nanomedicine for cancer. *Drug Discov Today*. 2012;**17**(1-2):71-80. doi: 10.1016/j.drudis.2011.09.009. PubMed PMID: 21959306. PubMed PMCID: PMC3259195.
32. Yallapu MM, Gupta BK, Jaggi M, Chauhan SC. Fabrication of curcumin encapsulated PLGA nanoparticles for improved therapeutic effects in metastatic cancer cells. *J Colloid Interface Sci*. 2010;**351**(1):19-29. doi: 10.1016/j.jcis.2010.05.022. PubMed PMID: 20627257.
33. Kumar B, Priyadarshi R, Deeba F, Kulshreshtha A, Kumar A, et al. Redox responsive xylan-SS-curcumin prodrug nanoparticles for dual drug delivery in cancer therapy. *Mater Sci Eng C Mater Biol Appl*. 2020;**107**:110356. doi: 10.1016/j.msec.2019.110356. PubMed PMID: 31761247.
34. Li F, Li X, Li B. Preparation of magnetic polylactic acid microspheres and investigation of its releasing property for loading curcumin. *Journal of Magne-*

- tism and Magnetic Materials*. 2011;**323**(22):2770-5. doi: 10.1016/j.jmmm.2011.05.045.
35. Yallapu MM, Othman SF, Curtis ET, Gupta BK, Jaggi M, Chauhan SC. Multi-functional magnetic nanoparticles for magnetic resonance imaging and cancer therapy. *Biomaterials*. 2011;**32**(7):1890-905. doi: 10.1016/j.biomaterials.2010.11.028. PubMed PMID: 21167595. PubMed PMCID: PMC3021632.
36. Wang N, Guan Y, Yang L, Jia L, Wei X, Liu H, Guo C. Magnetic nanoparticles (MNPs) covalently coated by PEO-PPO-PEO block copolymer for drug delivery. *J Colloid Interface Sci*. 2013;**395**:50-7. doi: 10.1016/j.jcis.2012.11.062. PubMed PMID: 23305884.
37. Cheng KK, Wang YX, Chow AH, Baum L. Amyloid plaques binding curcumin conjugated magnetic nanoparticles for diagnosis in alzheimer's disease tg2576 mice. *Alzheimer's & Dementia*. 2014;**10**(45):P152-3. doi: 10.1016/j.jalz.2014.04.122.
38. Mancarella S, Greco V, Baldassarre F, Vergara D, Maffia M, Leporatti S. Polymer-Coated Magnetic Nanoparticles for Curcumin Delivery to Cancer Cells. *Macromol Biosci*. 2015;**15**(10):1365-74. doi: 10.1002/mabi.201500142. PubMed PMID: 26085082.